Accepted Manuscript

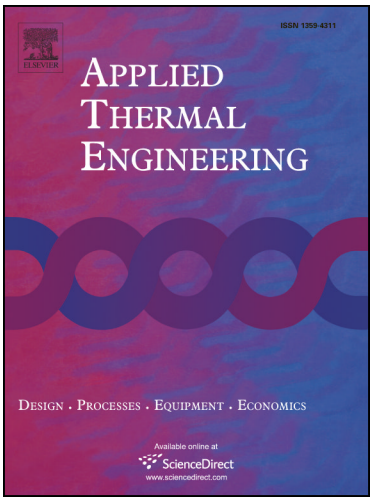

MARINE DIESEL ENGINE FAILURE SIMULATOR BASED ON THERMODYNAMIC MODEL

Jose Antonio Pagán Rubio, Francisco Vera-García, Jose Hernandez Grau, Jose Muñoz Cámara, Daniel Albaladejo Hernandez

PII: S1359-4311(18)31654-5
DOI: https://doi.org/10.1016/j.applthermaleng.2018.08.096
Reference: ATE 12599

To appear in: *Applied Thermal Engineering*

Received Date: 14 March 2018
Revised Date: 24 July 2018
Accepted Date: 27 August 2018

Please cite this article as: J. Antonio Pagán Rubio, F. Vera-García, J. Hernandez Grau, J. Muñoz Cámara, D. Albaladejo Hernandez, MARINE DIESEL ENGINE FAILURE SIMULATOR BASED ON THERMODYNAMIC MODEL, *Applied Thermal Engineering* (2018), doi: https://doi.org/10.1016/j.applthermaleng.2018.08.096

MARINE DIESEL ENGINE FAILURE SIMULATOR BASED ON THERMODYNAMIC MODEL

Jose Antonio PAGÁN RUBIO[1], Francisco VERA-GARCÍA[2], Jose HERNANDEZ GRAU[2], Jose MUÑOZ CÁMARA[2], Daniel ALBALADEJO HERNANDEZ[2].

[1]NAVANTIA, Diesel Engine Factory, Diagnose Center and Product Development. Cartagena, Spain.

[2]Universidad Politécnica de Cartagena, Escuela Técnica Superior de Ingeniería Industrial, Departamento de Ingeniería Térmica y de Fluidos, Cartagena, Spain.

Corresponding author: francisco.vera@upct.es

ABSTRACT

The diesel engine is a widely used machine in naval sector both as a propeller and auxiliary generator sets, being the most critical equipment of vessel platform. Therefore, diesel engine reliability optimization has a transcendental impact on vessel availability, safety and life cycle costs.

This article describes the development of a 4-stroke high speed marine diesel engine failure simulator used in military and civil vessels as the main engine of small patrols and yachts and as an auxiliary genset for larger vessels. Failure simulator is based on a one-dimensional thermodynamic model developed in AVLBoost©, adjusted and validated with experimental data from a real engine in a test bench.

The developed model is able to reproduce with confinable results the effect of a large number of typical thermodynamic failures, the behavior of the engine and the effects over several parameters measured and non-measured. Therefore, it is possible to obtain the engine response to failures without having to provoke them in real engine and also it is possible to know the symptoms of one failure before this failure becomes dangerous for the correct behavior of the engine. In addition, this paper exposes a methodology which allows to obtain a failure simulator of any marine diesel engine. This simulator is able to identify diesel engine symptoms under failure condition and build a reliable failure database for diagnosis purposes.

Keywords: diesel engine modeling, diesel engine simulation, failure detection, diagnosis.

HIGHLIGHTS

- Marine diesel engine characterization using experimental measurement.
- A one-dimensional thermodynamic model which faithfully represents the real engine behavior.
- Model used as a simulator of the 15 most typical marine diesel engine thermodynamic faults.
- Onboard detectable symptoms of diesel engine failures are analyzed and characterized.

1. INTRODUCTION

The diesel engine has a leading position in both propulsion and power generation in the naval sector. While the use of large 2-stroke engines is common in civil ships, military ships use 4-stroke engines due mainly to size restrictions. Low speed 2-stroke, medium speed 4-stroke are used for propulsion and medium or high-speed 4-stroke for auxiliary GENerator SETs (GENSETs), almost always turbocharged. The reason for diesel engine expansion in the naval sector is its high-power density, efficiency, reliability and better response to load changes compared to other solutions such as gas turbine [1, 2]. The relative low cost of acquisition of diesel engines is another important reason, but even more important is cost over the whole life cycle of the engine, taking into account that most of the total cost is operation and maintenance expenses [3]. However, although efficiency is important, the priority in defense is reliability, with the objective of maximizing vessel availability. A failure in the propulsion or power generation plant can constrain the achievement of the mission or prevent the ship from being available. In the worst case, it could put the safety of the crew at risk.

The maintenance has evolved from the more traditional based on corrective actions to current trends, increasingly focused on predictive actions [4] consequently has allowed to increase reliability of these engines. Predictive maintenance is based on monitoring the condition of equipment to detect when there is an anomaly and know when it is necessary to perform a maintenance action, instead of waiting for a breakdown or fulfill a certain number of operating hours.

In this scenario, a diagnosis system which is able to detect and diagnose failures that occur in a diesel engine before they become a catastrophic failure is a poweful tool to achieve the highest possible reliability. Diagnostic systems proposed in the literature can be classified among statistical, physical and hybrid / semi-physical systems [5]. The simplest statistical systems are based on limit values and trending monitoring. However, there is a large kind of sophisticated statistical and Artificial Intelligence (AI) algorithms [6, 7], where neural networks are the most frequently used [8]. Statistical and/or A.I. models require a large amount of reliable operating data (normal and failure) in order to obtain good results, as well as a lot of time for model training. On the other hand, physical systems (or models) are based on thermodynamic laws and modelling the processes inside of diesel engines [9]. These systems, although also need to obtain experimental data, but with a limited series of specific tests, is sufficient for engine model characterization and adjustment. Physical models have two important advantages. Firstly, a great variety of failures can be identified if the engine model is tested enough and adjusted. And secondly, these models can be adapted better to new environmental conditions, normally different from those tested in model training / adjustment, avoiding that these models produce false positives when the ship sails through very cold or warm climates. Thermodynamic model-based diagnosis systems proposed so far in the literature [10, 11] typically use both, operational data and in-cylinder pressure data. A large number of marine diesel engines do not monitor yet in-cylinder pressure despite their ability to show engine performance and condition, specially the smaller 4-stroke engines. This is due to the relatively high cost and short durability of this type of instrumentation. In these cases, this measurement is normally made using portable equipment to diagnose the engine after a long period in function. However, pressure monitoring trend is currently changing, especially for larger main propulsion engines. More and more of them adopt electronic control of fuel injection

and exhaust valves without camshafts. In these engines pressure monitoring is available from the manufacturer because it is necessary for control purposes. A significant number of such engines are already under operation in marine vessels. Nowadays, robust in-cylinder pressure adquisition systems begin to appear for real-time measurement where sensors do not have to be replaced before engine overhaul [12].

Therefore, it is possible to develop a mathematical model to be able to model the physical and thermodynamic processes inside of diesel engines [13] and, in consequence, to predict failures and diagnosis with better results than obtained with statistical / AI diagnosis whenever, unless a large amount of historical data (with and without failures) is available. The third and final approach are hybrid systems, which combine the advantages of physical models and statistical / AI models [6].

It is usual that, although a large number of historical data is available from an engine (or form a family of engines), only historical records of a very few typical failures that have occurred are usually obtained. Therefore, only a few failure modes can be characterized, unless there is a thermodynamic model that acts as a simulator of the engine [14] which obtains reliably failures symptoms not available with real data. Another option would be the introduction of these failures in a real engine [15] at test bench. However, this option is time consuming, requires high fuel consumption and the most important, safety of operators and engine will be compromised.

This paper describes the construction of a diesel engine model with the objective of good accurately reproducing the behavior of the engine both under normal conditions and in case of failure. Model is used as a virtual test platform to introduce failures and obtain the variation of important thermodynamic variables that represent the engine behavior.

To guarantee a good response and an accurate model, especially when failures are introduced, a one-dimensional wave action model is constructed using AVLBoost© v2016, widely used by the scientific community [16, 17, 18]. For the correct functioning of the model it has been necessary to use geometrical and real engine characteristic data, as well as to adjust and validate it using operational data obtained through experimental measurements in a test bench.

The most typical diesel engine failure modes that can be detected by thermodynamic parameters are simulated and, therefore, its response to failures introduced in the model can be known due to its thermodynamic response. Within the large number of variables the model can provide, the analysis has focused on the variables that are usually monitored on board. In this way it is possible to detect an early failure and solve the problem before it becomes catastrophic or avoid engine operation. In addition, some other variables, not usually monitored at present, have been taken into account and added to this study, because they have demonstrated to be good indicators of how the engine is working. In this way, all possible symptoms to be used in an engine diagnosis system would be identified according to results obtained in simulation.

2. METHODOLOGY

2.1 Model construction

2.1.1. Data collection

The first step to build the model is to follow appropriate steps to obtain and process needed engine data. In order to carry out this process, an organized and systematic procedure is designed [19]. This procedure specifies all the data required to carry out appropriate specific experimental measurement and to carry out pertinent calculations that allow obtaining all parameters the model needs. Table 1 shows general characteristics of the marine diesel engine used as an example to demonstrate proposed methodology. This is a 12 Vee 4-stroke high speed diesel engine with a rated power 1200kW@1800 rpm. It works at constant nominal speed since it works in a GENSET application and is one of the four GENSETS installed on board for power generation. Two turbochargers boost air pressure in two constant pressure air semi-manifolds. The air that comes from compressors is mixed and cooled in a single air cooler before air semi-manifolds. There are also two constant pressure exhaust gas semi-manifolds from which the gas flows into the turbines. Once all engine characteristic data have been collected, they are entered into a database [20] designed to store them in an organized and structured way. This database includes three types of data: general data, measurements and calculated data. This database, once it is filled in, will be a reference for the diesel engine under study and will be used to enter engine data in AVLBoost©.

Parameter	Value
Cycle	4 stroke
Number of cylinders	12V
Engine Rating ISO 3046/1 (25/25/1)	1200 kW
Engine speed	1800 rpm
Cylinder bore	165 mm
Stroke	185 mm
Compression ratio	15.5 : 1
Mean Effective Pressure	16.8 bar
Application	genset
Fuel	Marine Diesel Oil F76

Table 1. General specifications of marine diesel engine.

2.1.2. Experimental measurements

In addition to collecting geometric parameters, it is necessary to perform experimental measurements in a test bench. The measures to be carried out are defined in a specific test protocol that includes the typical parameters that are usually recorded during running and official tests for acceptance of a marine diesel engine and other additional parameters necessary to be able to characterize the engine for model building. Standard signals are monitored and registered by centralized test bench control system. However, additional measurements are carried out by portable equipment.

Engine performance tests are defined under standard conditions according to ISO 3046-1 [21]. Therefore, environmental conditions are recorded during tests in order to make appropriate corrections. Also, used engine fluids during tests, are authorized by engine designer, including F76 diesel fuel MIL-F-16884 [22].

Four days of trials of studied diesel engine and its generator, complete genset, are carried out with different environmental conditions. The tested points are 10%, 25%, 50%, 75% and 100% of nominal diesel declared power 1200 kW. These five test points are representative of the entire load range where the diesel engine will be operating on board. Engine operating speed is constant 1800 rpm because of its genset application.

Table 2 and Fig. 1 show the list of monitored parameters in test bench and position on the diesel engine. Parameters in Table 2 are numbered from *P1* to *P59* to identify measurement point on engine scheme shown in Fig. 1. These measurements made under controlled conditions at test bench are absolutely necessary for model development and adjustment. On the other hand, those parameters that are also monitored on-board in studied diesel engine are indicated in Table 2 with asterisk superscript.

Parameters have been obtained by direct measurement or calculated from one or more measured parameters. Table 2 indicates instrumentation used, measurements' precision and identifies calculated parameters.

An example of calculated parameters is that which indicates engine performance as corrected torque *P8*, corrected power *P9* and corrected specific consumption *P10*. *P8* and *P9* are obtained from engine speed *P1* and generator active power *P2* measurements using also generator efficiency and applying the correction according to standard conditions [21]. Other calculated parameters are specific fuel consumption *P10*, obtained from measured fuel consumption by fuel differential pressure at fuel tank and corrected power *P9*. Average exhaust gas temperature of each engine side is also calculated, being averaged outlet gas temperature bank A *P36* and averaged outlet gas temperature bank B *P37*. Air cooler pressure drop *P15* is obtained as the difference between pressures measured in air manifold *P14* and air cooler inlet *P12*.

Apart from standard parameters usually measured in an engine run-in, specific in-cylinder pressure and gaseous emissions measurements are made. In-cylinder pressure *P20*A is made in cylinder 1A. A synchronized measurement of the RPM and the Top Dead Center (TDC) with the in-cylinder pressure is necessary to obtain the last one. The TDC signal is corrected by a thermodynamic method before starting the measurements to obtain an accurated signal of the in-cylinder pressure. The process of treating dynamic pressure signals in the cylinder is described in [23]. Evolution of in-cylinder pressure along a thermodynamic cycle allows us to calculate the heat release law at which injected fuel burns [24]. Therefore, this signal is the basis for the combustion model integrated in engine thermodynamic model. IndicatorCal® is the in-cylinder pressure measuring system used, developed by Thermal and Fluid Engineering Department of the Universidad Politécnica de Cartagena [25].

Gaseous emission measurement is another additional measure that is not usually carried out but is also important to characterize the diesel engine. This measurement is made using a TESTO 360 analyzer. This measurement allows us to calculate the mass flow rates of air *P17* and gases *P21* as well as air / fuel ratio *P18*. An indirect method is used for O2 *P51*, CO2 *P52*, CO *P53*, NO *P54*, NO2 *P55* and NOx *P56* exhaust gas concentration measurements. Methodology used for measuring contaminating gases and calculating flowrates and emissions is indicated in ISO 8178 [26], which establishes a calculation based on fuel consumption and exhaust gas measurement analysis. This process made for studied diesel engine is described in [20].

Generator parameters are also recorded to have reference values of the complete genset although they are not shown in Table 2 or Fig. 1 since they are outside of this study scope. They also serve as a reference for comparison with those recorded in the vessel when the engine is in service.

Nº	Description	Unit	Instrument	Accuracy
P1	* Engine speed	rpm	Barber Colman 11200	±1% (FS)
P2	* Alternator Active Power	kW	Calculated	
P3	Fuel rack position	mm	LVDT position sensor	NA
P4	Fuel consumption tank differential pressure (inlet - outlet)	mbar	Siemens 7MF40331BA002RB6-Z	±0,82%
P5	* Fuel pressure	bar	Danfoss EMP2	±0,5% (FS)
P6	* Inlet fuel temperature	ºC	CMR PT100	±2 ºC
P7	Outlet fuel temperature	ºC	CMR PT100	±2 ºC
P8	Corrected engine effective torque	kNm	Calculated	
P9	Corrected engine effective power	kW	Calculated	
P10	Corrected fuel specific comsumption	g/kWh	Calculated	
P11	Air filter outlet aspiration pressure (bank A)	mmH2O	Water column	±0,1 mmH2O
P12	Cooler inlet air pressure (bank A)	bar	Danfoss EMP2	±0,5% (FS)
P13	Cooler inlet air temperature (bank A)	ºC	CMR PT100	±2 ºC
P14	* Intake manifold air pressure (bank A)	bar	Danfoss EMP2	±0,5% (FS)
P15	Air cooler pressure loss	mbar	Calculated	
P16	* Intake manifold air temperature (bank A)	ºC	CMR PT100	±2 ºC
P17	Air mass flow	kg/s	Calculated	
P18	Air-Fuel ratio (AFR)	kga/kgf	Calculated	
P19	Intake manifold air dynamic pressure (bank A)	bar	Kistler 6613	±0,5% (FS)
P20	In-cylinder dynamic pressure in cylinder Nº1 (bank A)	bar	Kistler 6061B	±0,5% (FS)
P21	Exhaust gas mass flow	kg/s	Calculated	
P22	Exhaust manifold gas dynamic pressure (bank A)	bar	Kistler 6613	±0,5% (FS)
P23	Indicate mean effective pressure (IMEP)	bar	Calculated	
P24	* Outlet exhaust gas temperature in cylinder Nº1 (Bank A)	ºC	Class1 K-Type Thermocouple	±1 %
P25	* Outlet exhaust gas temperature in cylinder Nº2 (Bank A)	ºC	Class1 K-Type Thermocouple	±1 %
P26	* Outlet exhaust gas temperature in cylinder Nº3 (Bank A)	ºC	Class1 K-Type Thermocouple	±1 %
P27	* Outlet exhaust gas temperature in cylinder Nº4 (Bank A)	ºC	Class1 K-Type Thermocouple	±1 %
P28	* Outlet exhaust gas temperature in cylinder Nº5 (Bank A)	ºC	Class1 K-Type Thermocouple	±1 %
P29	* Outlet exhaust gas temperature in cylinder Nº6 (Bank A)	ºC	Class1 K-Type Thermocouple	±1 %
P30	* Outlet exhaust gas temperature in cylinder Nº1 (Bank B)	ºC	Class1 K-Type Thermocouple	±1 %
P31	* Outlet exhaust gas temperature in cylinder Nº2 (Bank B)	ºC	Class1 K-Type Thermocouple	±1 %
P32	* Outlet exhaust gas temperature in cylinder Nº3 (Bank B)	ºC	Class1 K-Type Thermocouple	±1 %
P33	* Outlet exhaust gas temperature in cylinder Nº4 (Bank B)	ºC	Class1 K-Type Thermocouple	±1 %
P34	* Outlet exhaust gas temperature in cylinder Nº5 (Bank B)	ºC	Class1 K-Type Thermocouple	±1 %
P35	* Outlet exhaust gas temperature in cylinder Nº6 (Bank B)	ºC	Class1 K-Type Thermocouple	±1 %
P36	Averaged outlet exhaust gas temperature cylinders Bank A	ºC	Calculated	
P37	Averaged outlet exhaust gas temperature cylinders Bank B	ºC	Calculated	
P38	* Turbocharger inlet exhaust temperature (Bank A)	ºC	Class1 K-Type Thermocouple	±1 %
P39	* Turbocharger inlet exhaust temperature (Bank B)	ºC	Class1 K-Type Thermocouple	±1 %
P40	* Turbocharger outlet exhaust temperature (Bank A)	ºC	Class1 K-Type Thermocouple	±1 %
P41	* Turbocharger outlet exhaust temperature (Bank B)	ºC	Class1 K-Type Thermocouple	±1 %
P42	Turbocharger outlet exhaust pressure (bank A)	mmH2O	Water column	±0,1 mmH2O
P43	* Sea water pressure	bar	DANFOSS EMP2	±0,5% (FS)
P44	* Main cooler inlet sea water temperature	ºC	CMR PT100	±2 ºC
P45	Main cooler outlet sea water temperature	ºC	CMR PT100	±2 ºC
P46	* Main cooler inlet hot water temperature (engine outlet)	ºC	CMR PT100	±2 ºC
P47	Main cooler outlet hot water temperature (engine inlet)	ºC	CMR PT100	±2 ºC
P48	* Hot water pressure	bar	DANFOSS EMP2	±0,5% (FS)
P49	* Engine outlet lubricating oil temperature	ºC	CMR PT100	±2 ºC
P50	* Lubricating oil pressure	bar	DANFOSS EMP2	±0,5% (FS)
P51	O2 concentration dry in exhaust gas	%	TESTO 360 O2 analyser	-0,12% (FS)
P52	CO2 concentration dry in exhaust gas	%	TESTO 360 CO2 analyser	-0,45% (FS)
P53	CO concentration dry in exhaust gas	ppm	TESTO 360 CO analyser	-0,10% (FS)
P54	NO concentration dry in exhaust gas	ppm	TESTO 360 NO analyser	-0,44% (FS)
P55	NO2 concentration dry in exhaust gas	ppm	TESTO 360 NO2 analyser	-0,44% (FS)
P56	NOx concentration dry in exhaust gas	ppm	TESTO 360 NOx analyser	-0,44% (FS)
P57	* Engine room ambient temperature	ºC	TESTO 360 Temperature probe	±2 ºC
P58	* Engine room barometric pressure	bar	TESTO 360 pressure probe	±0,001 bar
P59	* Engine room relative humidity	%	TESTO 360 humidity probe	±3 %

NA: Not available

Key:

* Parameter monitorized onboard

Table 2. Monitored parameters at test bench.

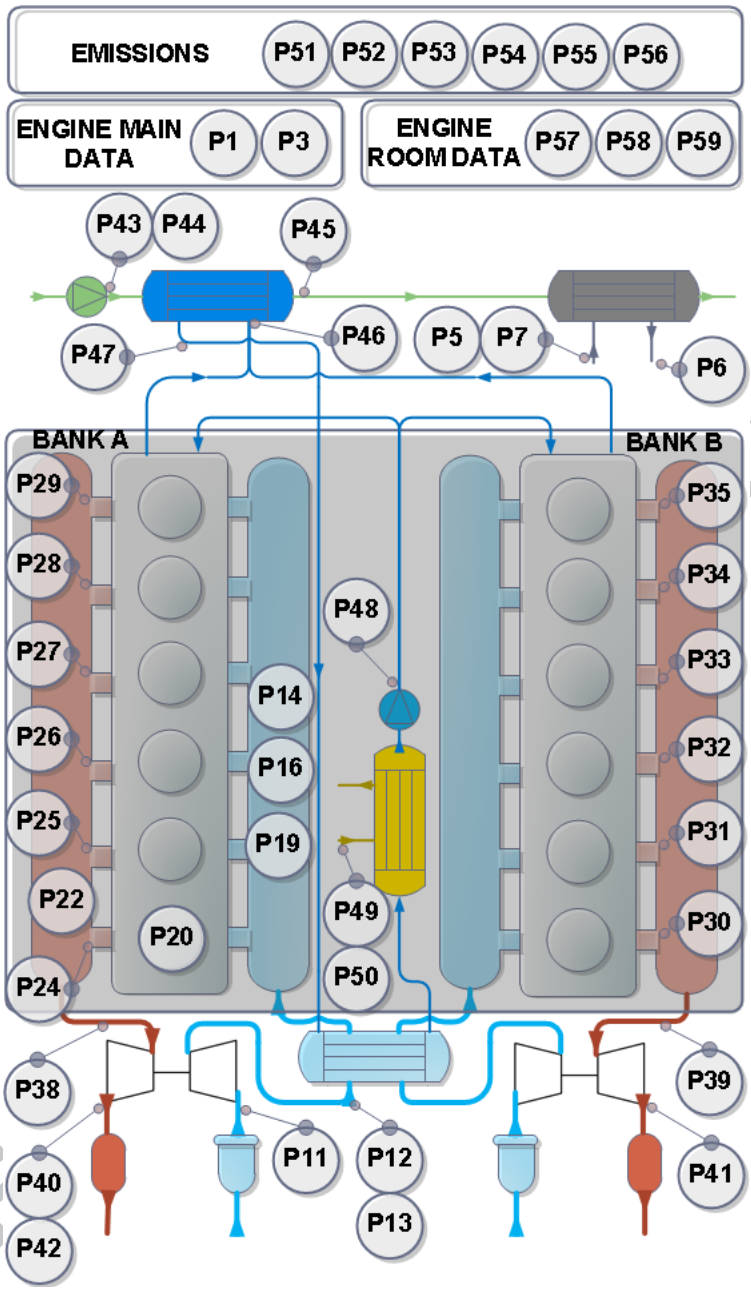

Fig. 1. Diesel engine points measured in test bench.

2.1.3. Model description

Once all necessary data has been collected, the model is built in AVLBoost©. This tool uses the conservation equations of mass, energy and momentum for modelling intake and exhaust collectors ducts. On the other hand, those equations are connected with contours conditions obtained from modelling of other engine components, like volumes, cylinder, turbocharger, valves or heat exchangers, each component has a special modelling to take into account the conservation equations and also the own special behaviour [27]. AVLBoost© is widely tested and used by a large number of authors. As an example, among many others, [16] models an EGR system of a diesel engine for NOx emission reduction, [17] develops an engine model that operates with biodiesel or [18] model an engine that uses gas. A detailed modelling process of marine diesel

engine is described at [28] and [29]. In the following paragraphs a brief description of the quality and general characteristics of the achieved model is presented.

This model simulates the thermodynamic cycle for a turbocharged four stroke engine destinated to marine services. The gas composition and thermodynamic properties in each element and instant is calculated by transport conservation equations [27]. According to this classical model, the mass Eq. (1), momentum Eq. (2) and energy Eq. (3) conservation equations for one-dimensional flow are:

$$\frac{\partial \rho}{\partial t} + \frac{\partial \rho u}{\partial x} = 0 \quad (1)$$

$$\frac{\partial \rho u}{\partial t} + u\frac{\partial \rho u}{\partial x} + \frac{\partial p}{\partial x} = 0 \quad (2)$$

$$\frac{\partial (\rho e\ )}{\partial t} + \left[\frac{\partial (\rho u h\ )}{\partial x}\right] = 0 \quad (3)$$

Where ρ is density, u velocity of fluid, t time, x flow longitudinal dimension, p pressure, e total internal energy and h total enthalpy. This equations system is used in conjunction with equation of state [24] considering an ideal gas.

The gas properties in each element and moment of time are calculated according to temperature, pressure and composition of mixture. A conservative criterion is established regarding the values recommended by AVLBoost© [30] to guarantee the quality of results. In particular, finite volume cell size is reduced from 30 to 20 mm and a convergence control is established in several elements. The simulation finishes when all convergence criteria are met for at least two engine cycles. Tolerance set in model elements is 100 Pa for averaged pressure and 0.1 K for averaged temperature.

The model takes into account the fuel properties [22], i.e. lower heating value and the stoichiometric air-fuel ratio. The same fuel is used in test bench and in the vessel.

Model main elements are identified in Fig. 2: air filters, compressors, air cooler, manifolds, cylinders and turbines, all connected by ducts. The engine configuration is modeled, taken into account the main characteristics, i.e. firing order A1-B2-A5-B4-A3-B1-A6-B5-A2-B3-A4-B6 and firing angle of each cylinder with respect to reference cylinder 1A, spatial distribution of cylinders, etc.

Monitored points at test bench and some others considered important because of their thermodynamic interest are also indicated in Fig. 2 with the code that is used in Table 2 and Fig. 1, including the turbocharger speed *TC RPM* which does not have a code assigned in Table 2 because it was impossible to measure in studied engine. In-cylinder pressure parameter *P20* is highlighted in green because it is one of the principal parameters used to evaluate engine behavior and also the accuracy of the resulting model.

Localized pressure losses in air filter before compressor and in exhaust duct and silencer located after turbine are modeled by a quadratic loss curve versus mass flow rate [27]. This curve is adjusted with pressure measurement after air filter *P11* for air filter and pressure drop after turbine with exhaust back pressure measurement *P42* for exhaust duct / silencer and introduced in the model as a local pressure drop.

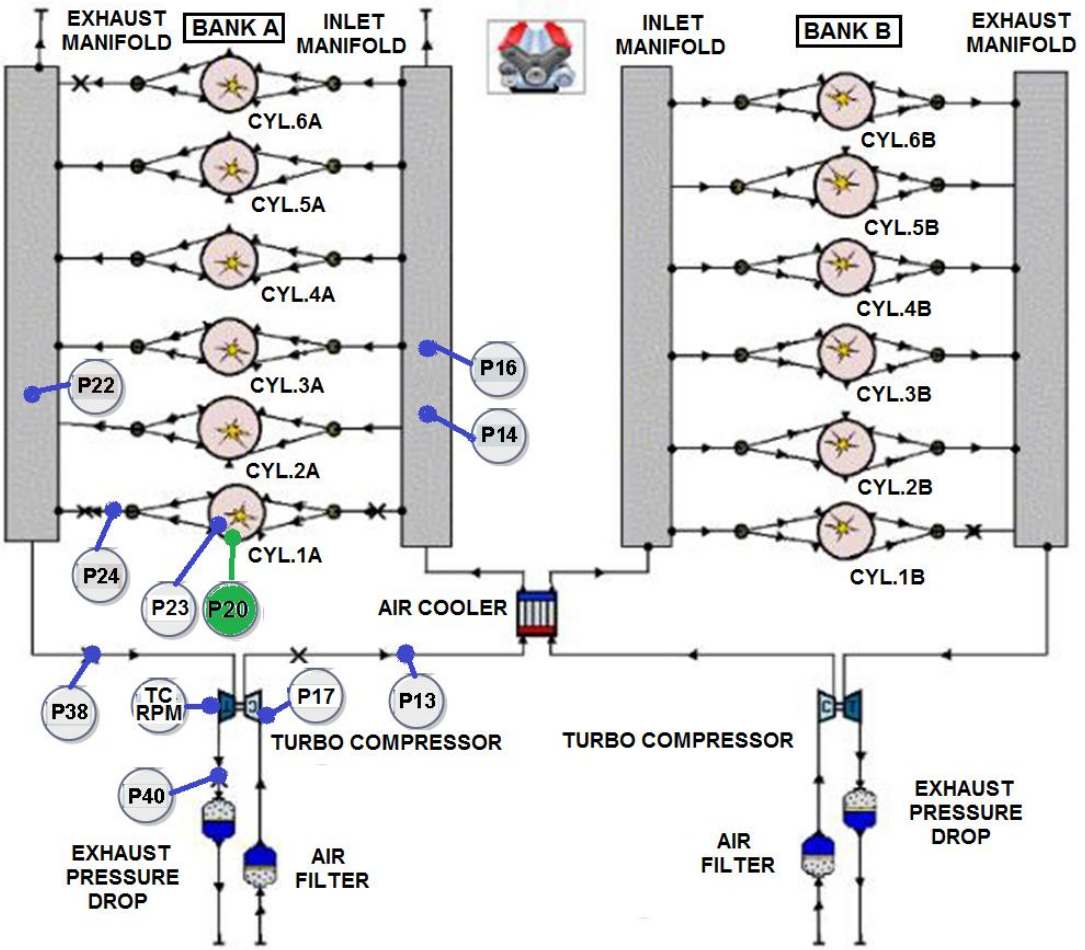

Fig. 2. AVL Boost © scheme of marine diesel engine model.

Elements that make up the model are joined by unidimensional ducts in order to be able to consider wave dynamics. One-dimensional flow is calculated by means of Euler continuity equations [27] through these conduits. Main ducts parameters are length, equivalent diameter, friction coefficient, wall temperature and others. Wall temperature in exhaust pipes is adjusted using cooling water temperature *P46* experimental values. On the other hand, exhaust and intake manifolds pipes are adjusted by means of an experimental measurement using a portable sensor.

Cuasi-stationary models are used for compressor and turbine of turbochargers. The complete turbine and compressor maps is introduced to ensure that turbocharging process responds to reality when changes in boundary conditions or when a failure condition is introduced in the model. SAE American Standard Code for Information Interchange (ASCII) text files to introduce map data according to SAE J1826 standard [31] is used.

For modelling the main air cooler, cooling capacity is defined from cooling water inlet temperature and cooler efficiency [27], and pressure drop in air cooler as a local drop depending of the air flow. The air cooler efficiency has been previously adjusted with water inlet *P47*, air inlet *P13* and air outlet *P16* temperatures measured at test bench, and pressure drop was adjusted by the same way as air filter previously explained.

Intake and exhaust manifolds have been modeled as fixed volumes calculated from real dimensions. Intake manifold heat transmission is considered negligible. However, heat transfer coefficient [32] in exhaust manifold has been adjusted to obtain experimental turbine inlet temperature of each operating point and engine side.

The cylinder model is the most complex and it is necessary to use several submodels to take into account all processes occurring inside: combustion, blow-by, mass flow rate and heat losses. Cylinders are defined from their basic dimensions, power train motion, combustion, heat transfer and mass flow renewal through intake and exhaust valves. Thermodynamic state in the cylinder is calculated with angular resolution by the first law of the thermodynamics equation and mass variation in cylinder [27]. It is established that internal energy in cylinder at each crankshaft angle is equal to the sum of piston work, fuel heat released, heat losses through the walls, energy difference of incoming and outgoing flows by valves, blow-by flow energy loss and fuel vaporization.

The combustion process is represented by the rate of heat release, modeled by a double Vibe law [33]. This model represents efficiently ignition delay, premixed and mixing-controlled combustion phases, typical combustion phases of marine diesel engines. Double vibe law is adjusted to reproduce heat release rate obtained from the in-cylinder pressure experimental measurements. This process is described in detail in [28] and [23].

Blow-by losses produced by gas that escapes from cylinder to crankcase is modeled considering an effective blow-by clearance [27] that corresponds to the gap between rings and jacket. This clearance and average pressure in crankcase are used to calculate instantaneous mass flow. This engine does not have pressurized crankcase, but there is a connecting duct from crankcase to compressor inlet. For this reason, crankcase atmospheric aspiration is established in blow-by model.

In order to model the mass flow in cylinder, laws of conservation are applied during the thermodynamic open cycle [27]. The lifting curves of intake and exhaust valves are used and their discharge coefficients to define cylinder filling and emptying.

Convective heat losses are simulated by Woschni heat transfer model [32]. Jacket heat exchange surface, combustion chamber and piston head, as well as the wall temperature data [27] are all entered in this model. Model has been adjusted by means of a convection loss factor in order to obtain experimental temperature in cylinder exhaust duct.

2.1.4. Model validation

Validation of the model is performed by comparing simulated and experimental mean values, turbocharger operating point and in-cylinder dynamic pressure.

Table 3 shows a comparison between mean values of performance and representative thermodynamic variables provided by simulation with respect to those measured in test bench.

	Operating points (% Load)							
	25		50		75		100	
Parameter	Measured	Simulated	Measured	Simulated	Measured	Simulated	Measured	Simulated
P14 Boost pressure (bar)	1.21	1.27	1.53	1.56	1.98	2.00	2.49	2.57
Error (%)		-5.00%		-2.00%		-1.00%		-3.20%
P17 Mass flow rate (kg/s)	0.38	0.40	0.49	0.50	0.62	0.66	0.78	0.85
Error (%)		-6.30%		-2.00%		-6.30%		-8.30%
P23 IMEP (bar)	5.18	6.04	9.84	9.83	14.47	14.22	18.93	18.82
Error (%)		-16.60%		0.10%		1.70%		0.60%
P22 Exhaust manifold pressure (bar)	1.25	1.26	1.38	1.45	1.62	1.73	1.97	2.11
Error (%)		-0.80%		-5.10%		-6.80%		-7.10%
P38 turbo inlet temperature (K)	682.00	680.00	791.00	788.00	865.00	862.00	932.00	930.00
Error (%)		0.30%		0.40%		0.30%		0.20%
P40 turbo outlet temperature (K)	652.00	652.00	732.00	737.00	778.00	782.00	807.00	817.00
Error (%)		0.00%		-0.70%		-0.50%		-1.20%

Table 3. Comparison between simulated and experimental mean values.

Table 3 indicates that model simulates engine behavior with a good precision. There is a general difference less than 5% between simulation and experimental values, although less precision in some parameter for low load operating points. This is due to the filter procedure to obtain the Heat Release Law from instantaneous pressure data, as it is detailing explained in congress communications [19] and [29].

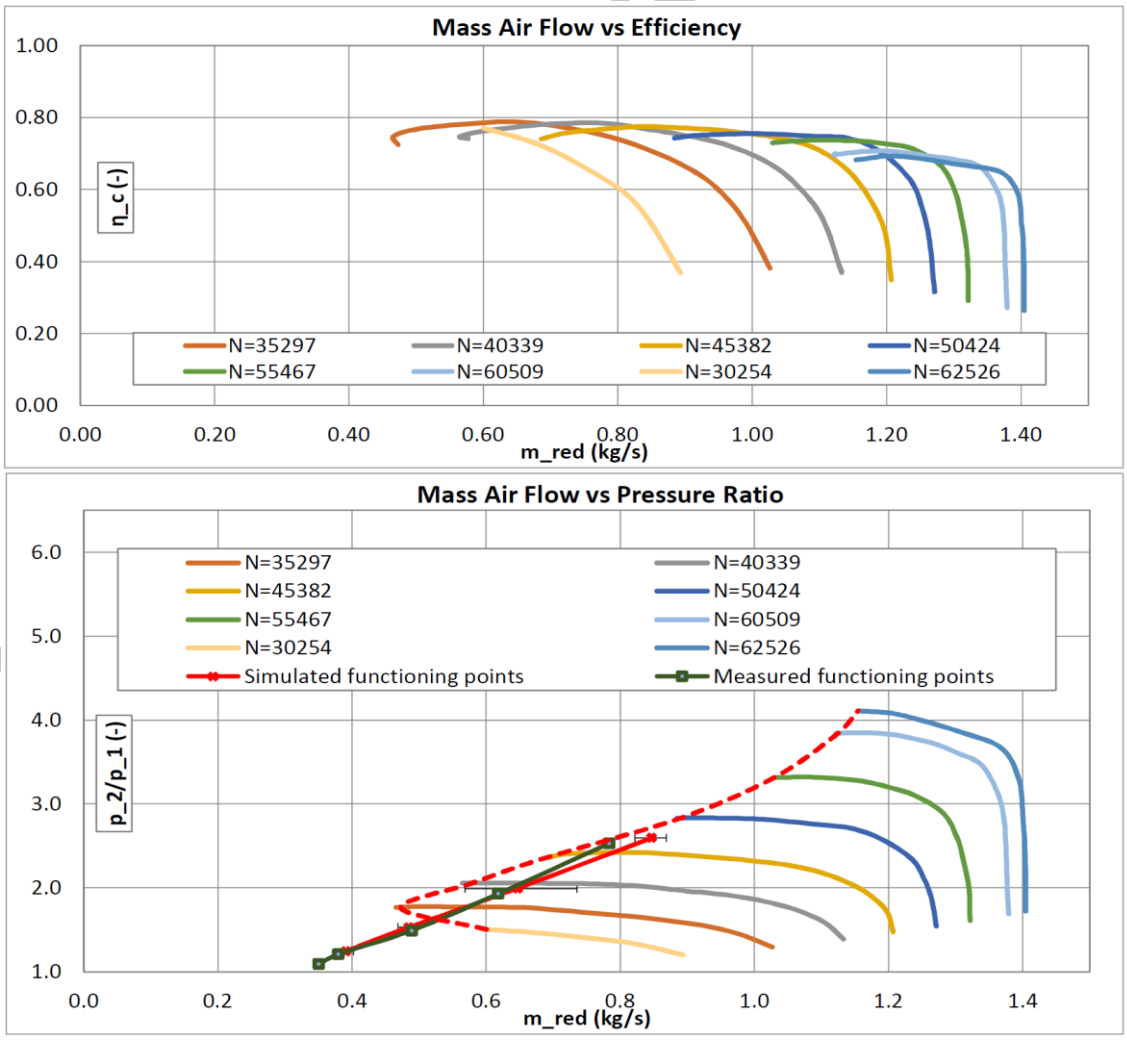

Fig. 3. Compressor map.

Fig. 3 shows engine operating points obtained experimentally and by modeling on the compressor map. Characteristic parameters represented on the compressor map are corrected speed, corrected mass flow rate, pressure ratio (total to total) and isentropic efficiency. Range of maximum and minimum mass flow rate available in the compressor has also been shown in order to assess whether compressor instantaneously works in surge zone when the engine moves between two load points. This figure indicates there is a high coincidence between real operating points and simulated ones. In addition, it is verified the turbocharger works in high performance area at medium and high load, although it is near surge line.

In addition to main values, validation of in-cylinder dynamic pressure is performed. Fig. 4 shows this measurement in cylinder 1A carried out in all loads compared to the same parameter obtained by simulation.

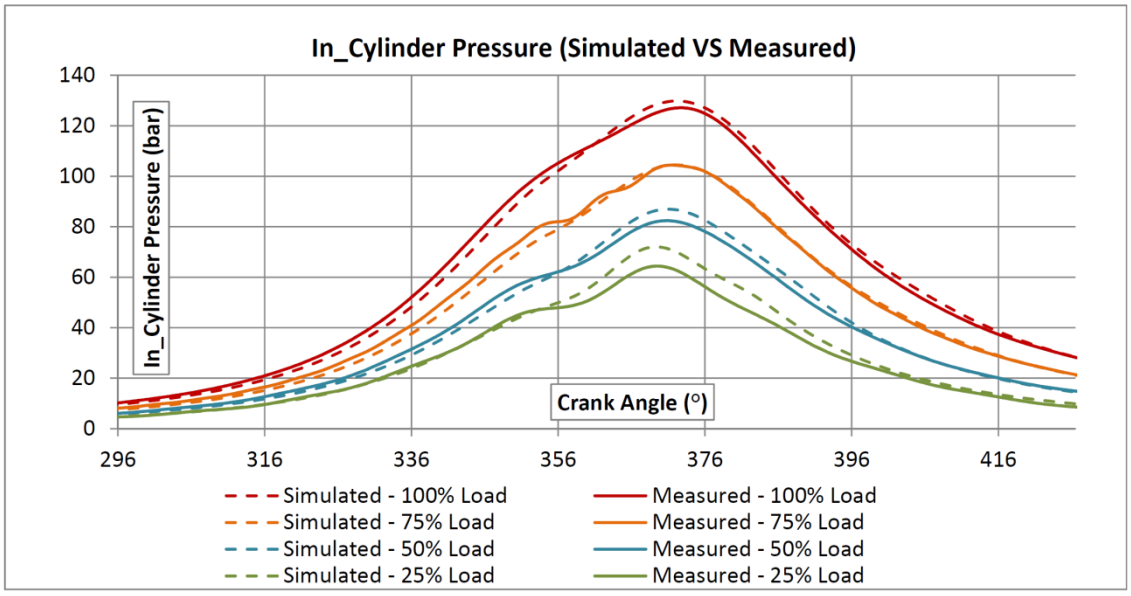

Fig. 4. Comparison between simulated and experimental in-cylinder pressure dynamic values.

The level of adjustment is observed between model and measurements for both main and instantaneous values is high. Therefore, it is considered that the model is adjusted and validated satisfactorily, so it is able to be used as a failure simulation platform without the need to produce them in a real diesel engine.

2.2. Failure simulation

Once the model has been adjusted and validated, failures are introduced one by one. In this work, a one-dimensional engine model is used; therefore, it takes into account the wave dynamics and its influence on cylinder mass flow rate. Each failure is introduced taking the precaution of provoking a range of reasonable and realistic variation of parameters that define failures. In [14] and [33] it is possible to find a similar work but using a 2-stroke marine diesel engine and with a simplest model and failure simulator.

This work describes how 15 of the most typical thermodynamic failures are reproduced, represented with the codes *F1* to *F15* [28]. Excessive pressure drop in air filter *F1*, efficiency reduction in air cooler *F2*, excessive pressure drop in air cooler *F3*, air compressor failure *F4*, intake air manifold leakage *F5*, intake valve seat failure *F6*, misfiring *F7*, excessive blow-by *F8*, failure of valve clearance adjustement - lower clearance- *F9*, failure of valve clearance adjustement - higher clearance - *F10*, injection timing failure – advance timing- *F11*, injection timing failure – delayed timing- *F12*, turbine failure *F13*, exhaust manifold leakage *F14*, excessive pressure drop in exhaust ducts *F15*.

It must be taken into account that described failures are simulated in a single element of the engine, that is, in a filter, in a compressor, in a turbine, in a half-manifold or in a cylinder. It has been proceeded this way since it usually happens like this in real conditions. Engine behavior would be different if a failure occurs in all elements of the same type. It can be expected that effects would be amplified by twelve if it occurs in all cylinders or by two if it does it in turbocharging systems. The same type of failure is unlikely to occur at various engine sites at the same time. What usually happens is it appears first in one element and this leads to another type of failure or, is transmitted by overstrain to other similar elements or other systems producing another failure. If initial failure is detected in time, it is very likely the failure is not spread. Thus, reliability is improved and engine maintenance is reduced during its useful life. At least two levels of failure intensity have been introduced for every failure mode in order to know engine response in both cases. The following sections describe in detail the procedure used for the introduction of each failure mode in this model.

2.2.1. Excessive pressure drop in air filter *F1*

Air filter pressure drop is a quadratic function of mass flow rate. The value of the constant, which multiplies this function for the pressure drop under normal operating conditions, is constant and considered as nominal value $a_{1,nom}$. To simulate when excessive obstruction, nominal value must be multiplied by K, with value 5 or 10 to simulate a small obstruction or a severe one respectively. Then, constant would be $a_{1,f}$, = K * $a_{1,nom}$ where (K = 5, 10). In this way pressure drop quadratic curve is readjusted according to the new value $a_{1,f}$.

This failure is introduced only in air filter located in side A of the engine, "AIR FILTER - BANK A" of Fig. 2. This failure may be caused by accumulated dust in air filter or other particles of suction air. If it is considered a failure as an important change in the "normal" operating conditions, in this case it would be, for example, the lack of filter replacement or cleaning in scheduled maintenance operations, or filter obstruction by an external agent.

2.2.2. Efficiency reduction in air cooler *F2*

Air cooler efficiency is simulated by a value that multiplies efficiency equation as a function of the mass flow rate and cooler inlet water temperature. These parameters have a different value for each engine load. In normal conditions, the equation is adjusted using constant $a_{2,nom}$.

Under failure condition, the value of efficiency is multiplied by a constant, K, which takes the value 0.5 or 0.75, depending on whether cooler efficiency reduction of 50% or 75% respectively from calculated value in adjusted equation. Thus, the value is affected according to the equation $a_{2,f} = K * a_{2,nom}$ (K=0.5, 0.75). This failure is simulated in the only air cooler of this engine, "AIR COOLER" of Fig. 2. It may be several failure causes, such as exchange area reduction, corrosion or other similar reasons that produce a reduction of cooling capacity. It is important to note that a failure of this type is accompanied by the failure described in the following section.

2.2.3. Excessive pressure drop in air cooler *F3*

In the same way to air filter pressure drop, the equation that defines normal pressure drop in the cooler is adjusted at nominal functioning point under normal conditions using a constant $a_{3,nom}$. In conditions of excessive obstruction, costant changes to $a_{3,f} = K * a_{3,nom}$ (K=5, 10). In this way the quadratic curve of pressure drop is readjusted according to the new value $a_{3,f}$. *F3* is simulated in the only air cooler, "AIR COOLER" in Fig. 2. This failure is caused by obstruction of air ducts by solid deposits or other obstruction agents.

2.2.4. Air compressor failure *F4*

Usually, this failure is considered by a compressor isentropic efficiency reduction as reflected in references [14] and [33]. In this work, an air mass flowrate reduction is also considered. Values of compressor isentropic efficiency and of air mass flowrate under normal conditions are $a_{4a,nom}$ and $a_{4b,nom}$ respectively. This failure is only simulated in the compressor located at side A of the engine, "TURBO COMPRESSOR - BANK A" of Fig. 2. In conditions of failure values isentropic efficiency and of air mass flowrate are $a_{4a,f} = K * a_{4a,nom}$ (K=0.5, 0.75) and $a_{4b,f} = K * a_{4b,nom}$ (K=0.5, 0.75) respectively. This failure is caused by dust accumulation and other rubbish in impeller or diffuser as well as damages that produce changes in geometry. Experience of the authors in compressor failure historic reports indicate there is normally geometric damage and dust or rubbish accumulation. This produces a loss in air mass flow rate and efficiency of the compressor, which is the reason why a reduction of air mass flowrate has been added. Although dirt can accumulate in both compressors at the same time, this is usually removed in routine maintenance tasks. In this study, it has been decided to simulate this failure only in one of them in order to be able to detect differences between air manifolds when this failure occurs.

2.2.5. Intake air manifold leakage *F5*

To simulate this failure, a 5 mm diameter tube is created without restrictions in intake manifold open to the atmosphere. The value of discharge coefficient of this tube under normal conditions is $a_{5,nom} = 0$, that is, there is no leakage and also does not affect the wave dynamics in air manifold. Under failure conditions, discharge coefficient is $a_{5,f} = a_{5,nom} + K$ (K=0.5, 1). There are no simulation references for this failure mode, however, this small loss is considered realistic. This failure is only simulated in side A air manifold, "INLET MANIFOLD - BANK A" of Fig. 2, because this is not what usually occurs simultaneously in both manifolds. Causes of this failure may be a lack of sealing by cracks in material or pipe joints connected to the air intake manifold.

2.2.6. Intake valve seat failure *F6*

This failure is modeled by modifying lifting curve in one of the cylinder 1A intake valves, "CYL.1A" of Fig. 2. Under normal conditions, lift value when the valve is closed is $a_{6,nom}$ = 0 mm. In conditions of failure lift when the valve should be theoretically closed is $a_{6,f} = a_{6,nom} + K$ (with K=0.5, 1). As *F5*, neither there are simulation references for this failure mode, anyway a maximum lift of 1 mm is considered enough. This failure is caused by accumulation of soot in the intake valves seating area. It is more common in intake valves where thermal stress is greater, also more probable in diesel engines that operate for a long time at low load. The failure in a single intake valve is considered to be the most realistic scenario.

2.2.7. Misfiring *F7*

The value of fuel mass flowrate under normal conditions is variable with engine load and considered as $a_{7,nom}$,. In failure conditions, the fuel mass flowrate is $a_{7,f} = K * a_{7,nom}$ (with K=0.75, 0.5), therefore, it is only simulated partial misfiring of 25% and 50% less fuel respectively than normal conditions for only cylinder 1A, "CYL.1A" of Fig. 2. The reason is because most of the times it is detected and repaired / replaced before getting to full misfiring. This failure can be caused by several reasons, such as clogging injector nozzle orifices, reduction of injection pressure, low quality fuel injection or other fuel system failures that reduce the quantity and / or quality of the fuel in injector.

2.2.8. Excessive blow-by *F8*

Excessive blow-by is produced when there is a cylinder compression ratio loss, mainly due to the clearance between piston rings and sleeve, defined as $a_{8,nom}$. This value determines blow-by useful area under normal conditions. In failure conditions, the value of clearance between rings and sleeve is increased by 0.05 and 0.1 mm, so $a_{8,f} = K + a_{8,nom}$ (K=0.05, 0.1 mm). Loss of compression by excessive blow-by is simulated only in cylinder 1A, "CYL.1A" of Fig. 2. This failure can be caused by abnormal wear of piston rings and / or by excessive wear of cylinder liner. In the case this failure occurs in all cylinders at the same time, i.e. piston rings not replaced according to scheduled maintenance plan, intensity of the symptoms would be much greater. It has simulated a single cylinder because it is much simpler to extrapolate effect when is extended. Also it gives the opportunity to detect effects when this failure appears in only one cylinder.

2.2.9. Failure of valve clearance adjustment - lower clearance - *F9*

Under normal conditions $a_{9a,nom}$ and $a_{9b,nom}$ are defined as the clearance between rocker arm and intake valves, and between rocker arm and exhaust valves respectively. In failure conditions, the clearance values are $a_{9a,f} = K * a_{9a,nom}$ (K=0, 0.5) and $a_{9b,f} = K * a_{9b,nom}$ (K=0, 0.5). Effect of these new clearances increase slightly valve opening time since clearance value between the rocker arm and the valves is reduced until it disappears.

2.2.10. Failure of valve clearance adjustment - higher clearance - *F10*

Analogous to the previous case *F9*, under normal conditions $a_{10a,nom}$ and $a_{10b,nom}$ are the clearance between rocker arm and intake valves, and between rocker arm and exhaust valves. Under failure conditions the clearance values are $a_{10a,f} = K * a_{10a,nom}$ (K=1.5, 2) and $a_{10b,f} = K * a_{10b,nom}$ (K=1.5, 2) respectively. Effect is a slight reduction in valve opening time, since cylinder valves are pushed later by rocker arm. Only cylinder 1A valves, "CYL.1A" of Fig. 2, are simulated. This failure has the same possible root causes as *F9*.

2.2.11. Injection timing failure – advance timing - *F11*

Parameter $a_{11,nom}$ is defined as combustion start angle used in double vibe law when the engine runs under normal conditions. Under advance timing failure condition, parameter $a_{11,nom}$ moves forward 2º or 4º, so $a_{11,f} = a_{11,nom} - K$ (K=2, 4). In this simulation it is supposed injection advance equal to combustion advance. This failure is simulated to only cylinder 1A, "CYL.1A" of Fig. 2, since this failure is usually caused by a mechanical mismatch in one injection pump high pressure element. An alternative timing simulation would have been to introduce the same failure to all cylinders at the same time. This could be possible if a mechanical adjustment error occurs in a relative position between injection pump shaft drive and crankshaft drive. As *F8*, failure in a single cylinder is considered more probable.

2.2.12. Injection timing failure – delayed timing - *F12*

Similar to the previous case, $a_{12,nom}$ is defined as combustion start angle used in double vibe law when the engine runs under normal conditions. In conditions of delayed timing failure, start angle is $a_{12,f} = a_{11,nom} + K$ (K=2, 4). This failure is analogous to *F11*, but in this case injection angle is delayed 2º or 4º. Failures *F11* and *F12* are separated because different symptoms are expected. Apart from different injection start angle, combustion law is usually different when injection is delayed or advanced. However, in this simulation, the same combustion laws are maintained because the engine has not been tested under these failure conditions.

2.2.13. Turbine failure *F13*

As in compressor failure *F4*, a reduction in turbine isentropic efficiency and mass flowrate are considered. Values of isentropic efficiency and mass flowrate under normal conditions are $a_{13a,nom}$.y $a_{13b,nom}$ respectively. This failure is only simulated in the turbine in side A, "TURBO COMPRESSOR - BANK A" of Fig. 2. In conditions of failure, value of isentropic efficiency and mass flowrate are $a_{13a,f} = K * a_{13a,nom}$ (K=0.5, 0.75) and $a_{13b,f} = K * a_{13b,nom}$ (K=0.5, 0.75) respectively. This failure is caused by accumulation of dirt and other rubbish in the nozzle and the impeller, as well as damages that cause changes in the geometry. A turbine failure is more frequent than in the compressor, due to the large concentration of dirt in the exhaust gases.

2.2.14. Exhaust manifold leakage *F14*

This failure is modeled by a small 5 mm diameter tube without any restrictions in the exhaust manifold open to the atmosphere, analogous to intake air manifold leakage *F5*. The value of discharge coefficient of this tube under normal conditions is $a_{14,nom} = 0$, therefore, there is no leakage. In failure conditions, discharge coefficient is $a_{11,f} = a_{11,nom} + K$ (siendo K=0.5, 1). Since there is no reference for this failure simulation, a small loss is expected for simulation. This failure is only simulated in side A exhaust manifold, "EXHAUST MANIFOLD - BANK A" of Fig. 2. This failure has similar reasons as *F5*.

2.2.15. Excessive pressure drop in exhaust ducts *F15*

To simulate this failure, exhaust manifold pressure drop is adjusted to a quadratic function that depends on the exhaust gas mass flowrate. The value of the constant, which multiplies this function for the pressure drop under normal operating conditions, is constant and considered as nominal value $a_{15,nom}$. Under conditions of excessive obstruction this constant will increase as $a_{15,f} = K * a_{15,nom}$ (K=5, 10). In this way quadratic curve of pressure drop is readjusted according to the new value $a_{15,f}$. This failure is caused by dirt accumulated after the turbine in exhaust ducts or other elements such as muffler/silencer.

3. RESULTS AND DISCUSSION

Once engine model has been validated and the 15 most typical thermodynamic failures introduced, failures simulation are carried out to analize the engine response. Simulation of failures is carried out in the same engine loads tested at test bench: 25%, 50%, 75% and 100% load. Execution time depends on the simulation case, but all cases needed approximately between 2-5 minutes using a common PC (Intel® Core™ i3-7130U CPU @ 2.70GHz – RAM 12 Gb).

Figures 5 and 6 show the effect of each failure over 10 thermodynamic parameters of interest. Those parameters have been chosen because they are monitored on board and usually they are symptoms of failure. In addition, other thermodynamic parameters have been analized, although are not usually measured since they are representative of engine performance. In the case that these new parameters are detected as good indicators, they could be obtained on board by direct or indirect measurements.

As a parameter representing performance, the Indicated Mean Effective Pressure (IMEP) has been selected. This is similar to provide the indicated power in aconstant speed engine like this one. All other parameters are operational. Here it is made an analysis by symptom, inlike in [14] where is made by failure. In this work is analyzed the variation that each parameter suffers in the fifteen failures to be able to easily compare its potential as a symptom that feeds to a database of failures. A failure diagnosis system [28] detects potential symptoms that are entries of a failure database. Diagnosis system does not know in advance which failure is causing active symptoms until such symptoms enter the failure database where combination of symptoms identifies the failure mode.

Results are presented as percentage variations with respect to their value under normal operating conditions and without any failure. Results are normalized and their effect can be directly compared among failures. The simulation not only contributes value to what parameters are affected by each failure, but also how much it influences each one of them. In addition, the simulation gives us the possibility to assess whether it is necessary to introduce a new parameter in the monitoring because it is very useful for the detection of one or several failures.

Figures 5 and 6 show variation of interesting parameters versus failures. X-axis shows the parameter variation in percentage with respect to normal value and Y-axis shows simulated failures. It is shown effectively that each failure has for each engine load and according to intensity of introduced failure. There are 4 vertical bars in each simulated failure, each of a different color. Color intensity indicates engine load. On the other hand, the vertical length of each bar is the variation of the parameter from a low intensity to a high intensity of the failure. A results discussion for each considered operating parameters is shown below.

3.1. Boost pressure behavior under failure condition *S1*

First graph of Fig. 5 shows the behavior of boost pressure *S1* under each simulated failure mode. It can be seen that this parameter is sensitive to almost all failures, except for cylinder valves clearance failures *F9* and *F10* where effect is almost zero. Intake pressure rises slightly in the event of a cooler efficiency failure *F2* and an increase when injection timing failure *F12*. On the other hand, boost pressure decreases if there is an excessive pressure drop in air cooler *F3*, intake valve seat failure *F6*, misfiring *F7*, excessive blow-by *F8*, turbine failure *F13* or mainly compressor failure *F4*, as would be expected in these types of failures. Boost pressure also decreases slightly when excessive pressure drop in air filter *F1*, intake air manifold leakage *F5*, exhaust manifold leakage *F14*, advanced timing injection *F11* and excessive pressure drop in exhaust ducts *F15*, but not so much. The sensitivity to almost all failures makes boost pressure an ideal indicator of failure detection, but in turn, it is difficult to distinguish which failure is happening by evaluating only this parameter variation. In order to distinguish between possible failures, it is necessary to cross with the effect over other parameters at the same time. This analysis will be dealt with later.

3.2. Air manifold temperature behavior under failure condition *S2*

The variation of air manifold temperature *S2* under every failure mode is shown in the second graph of Fig. 5. In this case, there is practically no variation in most failures. This parameter is mainly sensitive to cooler efficiency failure *F2* and to intake valve seat failure *F6*, rising significantly in both cases as expected. It is remarkable the fact that there is a strong rise of temperature when there is an admission valve seat defect by soot deposits. For all other failures, this parameter cannot be used as a direct indicator as there is no appreciable value change. However, it can be used as an excluding indicator, i.e. we can exclude failure *F6* within all failure possibilities if boost pressure is affected but air manifold temperature remains constant. This reasoning can be extended for the all indicators in which its effect is minimal.

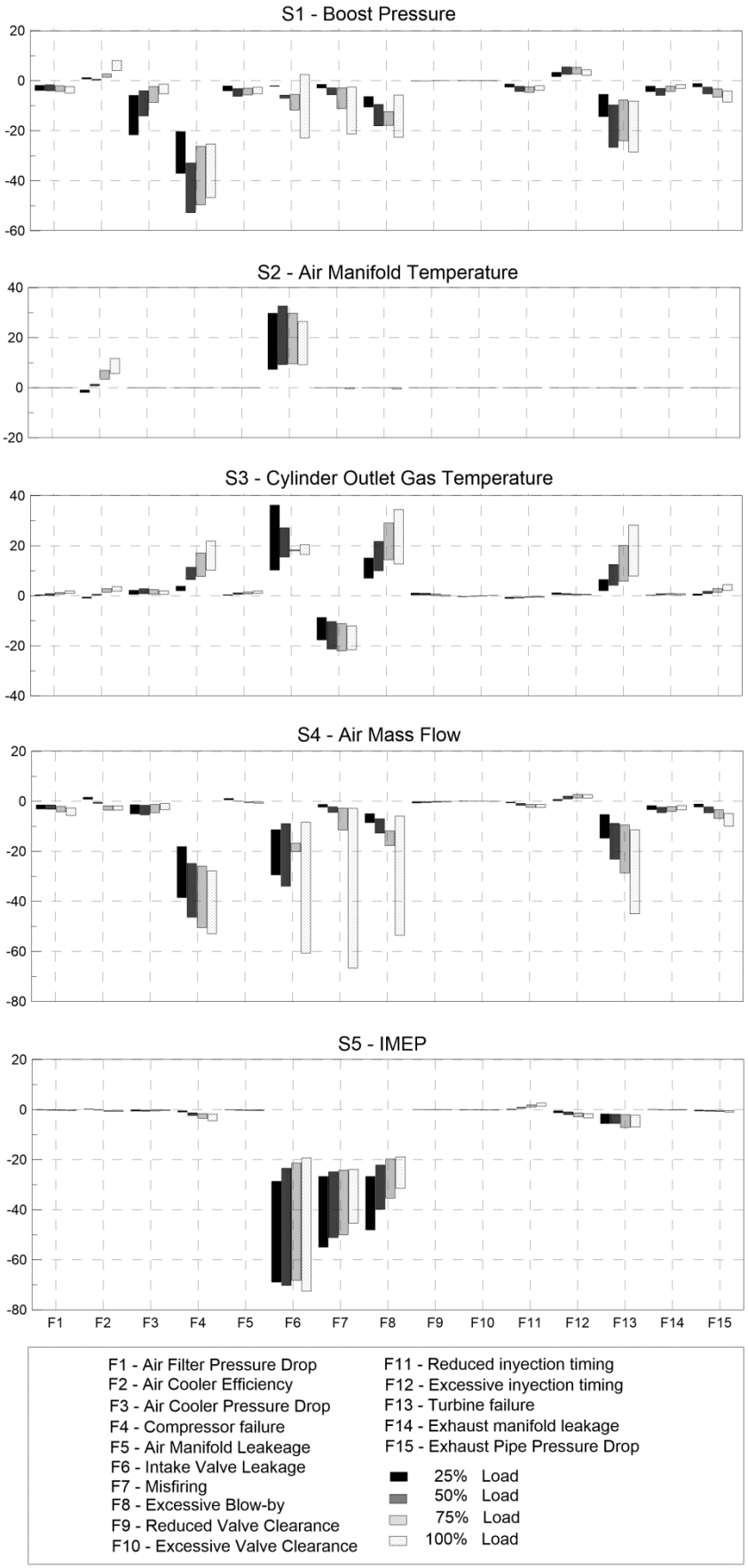

Fig. 5. Engine behaviour under simulated failures- 1 of 2.

3.3. Cylinder outlet gas temperature behavior under failure condition *S3*

Gas temperature behavior at cylinder outlet *S3* is shown in the third graph of Fig 5. It can be seen that this parameter increases significantly when air compressor failure *F4*, intake valve seat failure *F6*, excessive blow-by *F8* and turbine failure *F13*, increases slightly in the event of efficiency reduction in air cooler *F2* and excessive pressure drop in exhaust ducts *F15* and falls significantly if misfiring *F7* occurs. Misfiring produces a temperature reduction due to poor fuel pulverization and combustion in the cylinder. These cases occur when the unburned fuel in the cylinder is burned in the exhaust manifold near ~~to~~ the temperature sensor. These two phenomena have ~~got~~ the opposite effect in outlet gas temperature, so temperature variation ~~it~~ depends on injector state. Only when failure *F7* persists, and injector state gets worse, will gas temperature increase in exhaust manifold. This paper simulates the first phase of the injector failure before it drips. When it drips, combustion of the burnt fuel in the exhaust duct may occur outside the combustion chamber and therefore the sensor captures a temperature rise. This phenomenon should be taken into account when analysing the results. This parameter is in general a good failure indicator for turbocharging and cylinder problems. As in the previous case, effect of this parameter in combination with others can identify and / or exclude other type of failure.

3.4. Air mass flow behavior under failure condition *S4*

Variation of air mass flow in compressor *S4* under failure condition is shown in the fourth graph Fig. 5. It can be seen that this parameter falls severely when compressor failure *F4*, intake valve seat failure *F6*, misfiring *F7*, excessive blow-by *F8* or turbine failure *F13* and slightly when excessive pressure drops in air filter *F1*, cooler efficiency failure *F2*, excessive pressure drops in air cooler *F3*, exhaust manifold leakage *F14* or excessive pressure drops in exhaust ducts *F15*. It is remarkable that large falls, greater than 20-25%, happen only at high loads except before *F4* and *F6*, where it drops a lot even at partial loads. It is practically not sensitive to other failures, including a delay in the injection timing *F12*, which is the only case in which it rises, although almost negligibly. The important decrease effect of *F6* and *F8* demonstrates the importance of the absence of cylinder leaks. This parameter, apart from cylinder leaks, is a good indicator also for both, turbocharger and misfiring problems.

It is important to remark that mass flowrate is not usually identified as a symptom of any failure mode in the failure databases created by experience. According to simulation results, air mass flowrate would be a candidate indicator to be monitored on engine in order to improve failure prediction. A good strategy would be indirect on-line monitoring with checking periodically of direct monitoring off-line in order to verify that the indirect estimate is correct. This monitoring can be indirect, by means of a calculation from direct measurement of the pressure and the temperature in air manifold, or direct, measuring the air mass flow

3.5. IMEP behavior under failure condition *S5*

The behavior of IMEP *S5* under every failure mode is shown in the bottom graph of Fig. 7.5. This parameter has a similar reaction to mass air flowrate, although IMEP decreases much more under air compressor failure *F4* and/or turbine failure *F13*. IMEP also

decreases when there is an intake valve seat failure *F6*, misfiring *F7* or excessive blow-by *F8*, and it is more accentuated to partial loads. The results present a strong influence of mass flowrate over engine power, as it is expected. The other failures do not produce a significant alteration in IMEP, being between ± 0-3%, so this parameter would not be a good indicator of failure for those cases.

As air mass flow, IMEP is not identified as a symptom in failure databases created by experience. In order to include this parameter, it would be necessary to measure torque or measure instantaneous in-cylinder pressure. In the first case, it would be used together with an estimated value of engine mechanical efficiency obtained in the test bench. In the second case, processed in-cylinder pressure and analyses would obtain indicated parameters as IMEP. Currently there are real time in-cylinder pressure acquisition systems, although cost is high and only for high power propulsion engines is it quickly amortized. Therefore, it is a reasonable option to carry out a campaign of measurements periodically on the vessel, in a similar way to typical off-line data collection campaign for vibrations analysis. In-cylinder pressure offers a good idea of the engine state of health and it is a good indicator for great variety of failure related to injection process and engine combustion [34].

3.6. Turbocharger RPM behavior under failure condition *S6*

Variation of turbocharger speed *S6* under every mode is shown in the first graph of Fig. 6. It can be seen that this parameter falls significantly when there is a failure in compressor *F4* or in turbine *F13* and decreases moderately at low load and increases with higher engine load in the case of failure of intake valve seat failure *F6*, misfiring *F7* or excessive blow-by *F8*. This effect is mainly due to the turbine energy loss when these types of failure happen, either by flowrate reduction (leakages *F8* and / or intake reflows *F6*) or thermal energy exhausts reduction (less injected fuel *F7*). When there is leakage in exhaust manifold *F14* or excessive pressure drop in exhaust ducts *F15* decreases the turbocharger speed due to reduction of exhaust gas energy, the same reason explained above. This parameter is not very sensitive to the other failures. However, it does not remain completely invariable because any failure will translate into a change in engine and turbocharger energy distribution [34].

3.7. Compressor outlet temperature behavior under failure condition *S7*

Second graph of Fig. 6 shows the behavior of compressor outlet temperature *S7* under every failure mode. This parameter rises considerably when a compressor failure *F4* occurs due to the loss of its isentropic efficiency. It is also very sensitive to an intake valve seat failure *F6* due to the air reflux from the cylinder. On the other hand, it rises slightly when there is excessive pressure drop in air filter *F1*, efficiency reduction in air cooler *F2* or injection timing failure – delayed timing - *F12*. Also, this parameter drops significantly if misfiring *F7*, excessive blow-by *F8* or turbine failure *F13* occurs and go down smoothly when there is intake air manifold leakage *F5*, exhaust manifold leakage *F14* or excessive pressure drop in exhaust ducts *F15*. For the rest of failures, although there is a slight variation in most of them, it is too small to be used as a failure indicator.

Compressor output air temperature is not identified as a symptom of any failure mode in failure database created by experience, like the mass flowrate or the in-cylinder

pressure. But according to simulation results, it is a parameter that can give a lot of information about the possible failures that may occur in studied engine in combination with other parameters affected. Therefore, this signal is interesting to add to the engine measurement chain on board to improve diagnostic capability.

3.8. Exhaust manifold pressure behavior under failure condition *S8*

The variation of exhaust manifold pressure *S8* under every failure mode is shown in the third big graph of Fig. 6. It can be seen that this parameter increases until near to 120% of its nominal value when there is a turbine failure *F13* due to its direct relationship to turbine flowrate and efficiency. On the other hand, exhaust manifold pressure increases only slightly if there is excessive pressure drop in exhaust ducts *F15* because this failure affects more to turbine enery reduction. As expected, this parameter decreases significantly when there is a failure of the compressor *F4*, intake valve seat failure *F6*, misfiring *F7* or excessive blow-by *F8* due to engine flowrate reduction. Also, exhaust manifold pressure decreases slightly if there is an excessive pressure drop in air cooler *F3* or leakage in exhaust manifold *F14* because these failures reduce the engine massflow rate. This parameter, like boost pressure, is very sensitive to a large part of types of failure. It is necessary to remark that a failure in turbine has been modeled as a reduction in two coefficients, one that affects efficiency and another that affects flowrate. A flowrate reduction has an important effect over exhaust manifold pressure.

3.9. Turbocharger inlet temperature behavior under failure condition *S9*

The next to last bottom graph of Fig. 6 shows the behavior of turbocharger inlet temperature of side A *S9*. It can be seen that this parameter rises significantly when there is a compressor failure *F4*, intake valve seat failure *F6* or turbine failure *F13*. Variation is lighter if there is an efficiency reduction in air cooler *F2* or excessive blow-by *F8*. In addition, it is appreciable a very soft descent under misfiring *F7* and very soft rise if there is excessive pressure drop in exhaust ducts *F15*. However, the maximum variation of these two last cases does not reach 4%, which is not considered enough to be a robust indicator for these two failures. It is not very sensitive to other failures.

3.10. Turbocharger outlet temperature behavior under failure condition *S10*

The bottom graph of Fig. 6 shows the effect of every failure mode over turbocharger outlet temperature of side A *S10*. It can be seen that this parameter has a behavior almost identical to turbocharger inlet temperature for similar failures. The only small difference between the both is that outlet temperature increases at a slightly higher percentage relatively to nominal values under failures. This is because the nominal value of this parameter is significantly lower and therefore its relative value to failures is higher. This effect makes it more sensitive and useful when detecting failures.

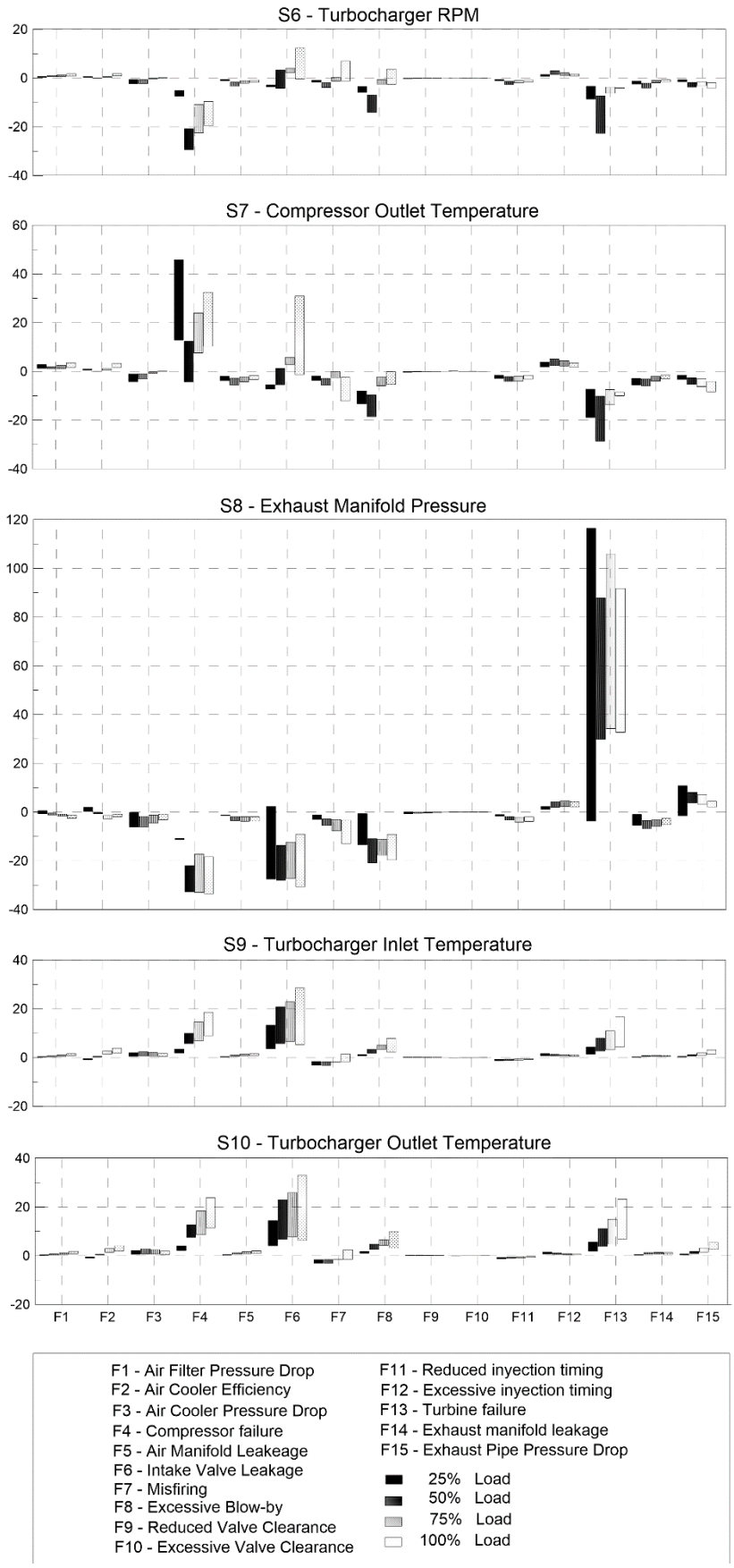

Fig. 6. Engine behaviour under simulated failures- 2 of 2.

3.11. Discussion of failure simulation results

Table 3 shows a summary of the relative effects on parameters value monitored in this work (or proposed to be monitored) produced in every of 15 simulated types of failures. In this table, signs (-) or (+) are used to indicate when a parameter goes down or rises with respect to its value under normal operating conditions. In addition, intensity of the parameters variation is shown in the following way: (-) / (+) small, (--) / (++) medium or (---) / (+++) for high intensity.

It is observed in Table 3 that all failures could be detected by one or more indicators except failures *F9* and *F10*. This is because parameters value that regulates these two failures is very low so it has almost no effect on the engine distribution diagram. Therefore, there is a very smooth cylinder valves lifting variation. Larger changes in these model parameters could be introduced, $a_{9a,f}$ y $a_{10a,f}$, to simulate these failures. However, it would not be realistic since cylinder valves clearance is periodically checked in programmed maintenance tasks. Therefore, a typical failure in valve regulation has not enough effect on on-board monitored parameters and, therefore, is not detectable.

In contrast, the engine model shows other failures do produce thermodynamic effects with detectable variations that can be detected using the appropriate indicators. An indicator / parameter alone it is usually a symptom of several possible types of failure. Nevertheless, if all the indicators are used at the same time, it is possible to find a unique combination of symptoms that allows its unequivocal identification of type of failures respect to the rest.

	Padm	Tadm	Tscil	m_{adm}	IMEP	nturbo	Tsc	Pesc	Tet	Tst
F1							+		+	+
F2	+	++					+		+	+
F3	--						-	-	+	+
F4	---		++	---	-	---	+++	---	++	+++
F5	-					-	--		+	+
F6	--	+++	+++	---	---	+/-	+++	---	+++	+++
F7	--		--	---	---	+/-	-	-	+/-	+/-
F8	--		+++	---	---	+/-	--	--	+	+
F9										
F10										
F11	-				+	-	-	-		
F12	+				-	+	+	+		+
F13	---		+++	---	-	--	---	+++	++	++
F14	-					-	-	-	+	+
F15	-			-		-	-	+		+

Key:
Intensity of effect --- -- - +/- + ++ +++

Table 4. Summary of engine parameters variation under failure conditions.

4. CONCLUSIONS

In this work, the process of a characteristic data collection has been followed. Experimental measurements in a test bench, experimental results analysis, recompilation of geometrical information, etc. have allowed to built, to adjust and to validate a reliable model of an engine. The following conclusions can be made:

- About model, it is possible to say that it represents realistically behavior of the engine with deviation between 2% and 5%. Therefore it can be said that the model is well adjusted globally. In addition, the comparison between experimental and modeled dynamic in-cylinder values offers a high concordance between them.
- An important conclusion of this work, is that a thermodynamic model has been achieved which reproduces engine behavior not only under normal conditions but also under failure conditions.
- Most of simulated engine responses under failure condition match with those set by the experts in a Failure Mode, Effects, and Criticality Analysis (FMECA) database [28]. On the other hand, there are occasions when response of a parameter is higher or lower than estimated by the experts' experience. An example of this is the simulated response to a valve regulation failure, which is lower than expected and predicted by the experts. However, other failures, such as a small inlet valve seat defect, affect engine parameters much more than experts' estimation [28]. Failures introduction and their analysis of engine's response has been carried out over a validated model.
- It is possible to say that this simulation platform allows to know efficiently how each type of failure affects over the engine behavior, so it provides valuable information both for design and maintenance, avoiding to provoke failure over the real engine to obtain data.
- This methodology with modelling tools allows detecting problems before they are increased to become catastrophic, and also optimize the operation of the engine before carrying out experimental tests on prototype, which reduces costs greatly.
- About the results, parameters like exhaust pressure, boost pressure, air mass flowrate and turbocharger speed are sensitive to a large type of failure but different intensity. In addition, other parameters are only sensitive to one or two types of failures.
- It is possible to find a unique combination of symptoms that allows its unequivocal identification of a type of 15 analysed failures.
- Following the methology and taking all theses criterions into account, it could be built, updated and improved a FMECA failure database in order to improve ability to diagnose diesel engine failures.

5. ACKNOWLEDGMENTS

This work has been done thanks to Navantia test bench facilities and technical guidance from the Universidad Politécnica de Cartagena both for measurements definition and engine thermodynamic modeling.

6. REFERENCES

[1] Royal Academy of Engineering: Future ship powering options – (2013) "Exploring alternative methods of ship propulsion", Report, https://www.raeng.org.uk/publications/reports/future-ship-powering-options.

[2] Haight, B.: (2013) "Marine Propulsion Order Survey, Diesel and Gas Turbine Worldwide", https://dieselgasturbine.com/wp-content/uploads/2016/06/2013WW_MPOS.pdf.

[3] Robert W. Button, Bradley Martin, Jerry Sollinger, Abraham Tidwell, (2015) "Assessment of Surface Ship Maintenance Requirements", ISBN: 978-0-8330-9253-3.RAND Corporation.

[4] Andrew K.S. Jardine, Daming Lin, Dragan Banjevic, (2006) "A review on machinery diagnostics and prognostics implementing condition-based maintenance", Mechanical Systems and Signal Processing, Volume 20, Issue 7, October, Pages 1483-1510, https://doi.org/10.1016/j.ymssp.2005.09.012.

[5] Anupam Das, J. Maiti, R.N. Banerjee, (2012) "Process monitoring and fault detection strategies: a review", International Journal of Quality & Reliability Management, Vol. 29 Issue: 7, pp.720-752, https://doi.org/10.1108/02656711211258508.

[6] Rolf Isermann, (2005) "Model-based fault-detection and diagnosis – status and applications", Mechanical Annual Reviews in Control, Volume 29, Issue 1, Pages 71-85, https://doi.org/10.1016/j.arcontrol.2004.12.002.

[7] Jacobo Porteiro, Joaquín Collazo, David Patiño, José Luis Míguez, (2011) "Diesel engine condition monitoring using a multi-net neural network system with nonintrusive sensors", Applied Thermal Engineering, Volume 31, Issues 17–18, Pages 4097-4105, ISSN 1359-4311, http://dx.doi.org/10.1016/j.applthermaleng.2011.08.020.

[8] Oihane C. Basurko, Zigor Uriondo, (2015) "Condition-Based Maintenance for medium speed diesel engines used in vessels in operation", Applied Thermal Engineering, Volume 80, Pages 404-412, ISSN 1359-4311, http://dx.doi.org/10.1016/j.applthermaleng.2015.01.075.

[9] Suneel Kumar, Manish Kumar Chauhan, Varun, (2013) "Numerical modeling of compression ignition engine: A review", Renewable and Sustainable Energy Reviews, Volume 19, Pages 517-530, https://doi.org/10.1016/j.rser.2012.11.043.

[10] D.T. Hountalas, A.D. Kouremenos, (1999) "Development and application of a fully automatic troubleshooting method for large marine diesel engines", Applied Thermal Engineering 19, 299±324, ISSN : 1359-4311.

[11] V.T. Lamaris, D.T. Hountalas, (2010) "A general purpose diagnostic technique for marine diesel engines – Application on the main propulsion and auxiliary

diesel units of a marine vessel", Energy Conversion and Management. 51(4). 740-753. 10.1016/j.enconman.2009.10.031.

[12] Rafal Pawletko, Stanislaw Polanowski, (2014) "Evaluation of current developments and trends in the diagnosis of marine diesel engines based on the indicator diagrams analysis", Journal of KONES Powertrain and Transport, Vol. 21, No. 4, DOI: 10.5604/12314005.1130492.

[13] M. Lapuerta, O. Armas, J.J. Hernández, (1999) "Diagnosis of DI Diesel combustion from in-cylinder pressure signal by estimation of mean thermodynamic properties of the gas", Applied Thermal Engineering, Volume 19, Issue 5, Pages 513-529, ISSN 1359-4311, http://dx.doi.org/10.1016/S1359-4311(98)00075-1.

[14] Dimitrios T Hountalas, (2000) "Prediction of marine diesel engine performance under fault conditions", Applied Thermal Engineering, Volume 20, Issue 18, Pages 1753-1783, https://doi.org/10.1016/S1359-4311(00)00006-5.

[15] Andrew J. Bayba, David N. Siegel, Kwok Tom, (2012) "Application of Autoassociative Neural Networks to Health Monitoring of the CAT 7 Diesel Engine", Army Research Laboratory, ARL-TN-0472.

[16] Zhu Jian, Ren Hongjuan, Luo Yiping, (2015) "Simulation Research on EGR Reducing NOX Emission of Diesel Engine", International Journal of Energy and Power Engineering, 2015; 4(5): 275-279, Published online October 14, DOI: 10.11648/j.ijepe.20150405.16.

[17] C. Iclodean, N. Burnete, (2012) "Computer simulation of ci engines fuelled with biofuels by modelling injection iRate law", Research Journal of Agricultural Science, 44 (1), pp. 249-257.

[18] Teuku Firsa et al, "AVL Boost Simulation of Engine Performance and Emission for Compressed Natural Gas Direct Injection Engine", Journal of Energy & Environment, 6 (1), 2014, pp. 1-3. ISSN 1985-7462.

[19] J. A. Pagán, F. Vera-García, J. Hernández Grau, (2015) "Proceso obtención medidas experimentales y tratamiento de datos para modelado motor diesel marino", IX Congreso Nacional de Ingeniería Termodinámica, 2015, URI: http://hdl.handle.net/10317/4709.

[20] J. Serra, (2016) "Desarrollo de base de datos de parámetros de un motor diésel rápido marino auxiliar a partir de medidas de ensayos, válido para análisis de prestaciones y diagnosis", TFG Grado en Arquitectura Naval e Ingeniería de Sistemas Marinos, Escuela Técnica Superior de ingeniería Naval y Oceánica, Universidad Politécnica de Cartagena.

[21] ISO 3046-1, (2002) "Reciprocating internal combustion engines - Performance - Part 1: Declarations of power, fuel and lubricating oil consumptions, and test methods -- Additional requirements for engines for general use".

[22] MIL-F-16884J: (1995) "Military specification fuel, naval distillate, F-76".

[23] J.Hernandez Grau, (2007) "Tratamiento Señal de Presión en Cilindro de Motores Diesel Marinos de Media Velocidad Medidas desde Válvula de Purga". Informe Interno UPCT – NAVANTIA.

[24] J.B. Heywood, Internal Combustion Engine Fundamentals. McGraw - Hill Book Company, ISBN 0-07-100499-8, 1988. 386-388 pp.

[25] J.Hernandez Grau, A. Muñoz, (2012) "IndicatorCal - Software de Adquisición y Tratamiento de Señales de Presión en Cilindro de Motores de Combustión Interna Alternativos", Trabajo no publicado.

[26] ISO 8178, (2006) "Reciprocating internal combustion engines – Exhaust emission measurement – Part 3: Definitions and methods of measurement of exhaust gas smoke under steady – state conditions".

[27] AVL BOOST Theory Reference, v2016.

[28] J.A. Pagan, (2017) "Sistema de diagnosis de motor diesel marino basado en modelo termodinámico e inteligencia artificial", Tesis doctoral, Universidad Politécnica de Cartagena, https://www.researchgate.net/profile/F_Vera-Garcia/publication/318674337_Sistema_de_diagnostico_de_motor_diesel_marino_basado_en_modelo_termodinamico_y_de_inteligencia_artificial/links/59772ed2458515e26d2cde9f/Sistema-de-diagnostico-de-motor-diesel-marino-basado-en-modelo-termodinamico-y-de-inteligencia-artificial.pdf.

[29] J. A. Pagán, J. Muñoz, F. Vera-García, J. Hernández Grau, (2016) "Ajuste de un modelo termodinámico unidimensional para simulación de fallos de motor diésel marino", IV Congreso nacional de I+D en defensa y seguridad, DESEID-2016-057, 2016, http://www.deseid.org/sites/default/files/documents/DESEID2016_LIBRO_ACTAS.pdf.

[30] AVL, BOOST: "User's Guide v2016".

[31] J1826_199503 Standard, "Turbocharger Gas Stand Test Code", SAE International, 1995.

[32] G. Woschni, (1967) "A Universally Applicable Equation for the Instantaneous Heat Transfer Coefficient in the Internal Combustion Engine", Society of Automotive Engineers Trans., Vol. 76, SAE paper 670931, pp. 3065.

[33] H.M. Nahim et al, "Oriented review to potential simulator for faults modeling in diesel engine", JASNAOE, Journal of Marine Science and Technology, 2015. DOI: 10.1007/s00773-015-0358-6.

[34] Peter Obrecht, "Diagnosis at marine diesel engines based on indicator cock pressure data", CIMAC World Congress on Combustion Engine, 2010.

7. CAPTION OF FIGURES

8. CAPTION OF TABLES

9. NOMENCLATURE

Acronyms

General acronyms

AI	Artificial Intelligence
FMECA	Failure Mode, Effects, and Criticality Analysis
GENSET	GENerator SET
IMEP	Indicated Mean Effective Pressure
ISO	International Organization of Standarization
SAE	Society of Automotive Engineers
TC RPM	Turbocharger Speed
TDC	Top Dead Center

Parameters monitored in test bench

P1	Engine speed
P2	Alternator Active Power
P3	Fuel rack position
P4	Fuel consumption tank differential pressure (inlet - outlet)
P5	Fuel pressure
P6	Inlet fuel temperature
P7	Outlet fuel temperature
P8	Corrected engine effective torque
P9	Corrected engine effective power
P10	Corrected fuel specific comsumption
P11	Air filter outlet aspiration pressure (bank A)
P12	Cooler inlet air pressure (bank A)

P13	Cooler inlet air temperature (bank A)
P14	Intake manifold air pressure (bank A)
P15	Air cooler pressure loss
P16	Intake manifold air temperature (bank A)
P17	Air mass flow
P18	Air-Fuel ratio (AFR)
P19	Intake manifold air dynamic pressure (bank A)
P20	In-cylinder dynamic pressure in cylinder Nº1 (bank A)
P21	Exhaust gas mass flow
P22	Exhaust manifold gas dynamic pressure (bank A)
P23	Indicate mean effective pressure (IMEP)
P24 to P35	Outlet exhaust gas temperature in cylinder Nº1 to Nº6 (Bank A) & cylinder Nº1 to Nº6 (Bank B)
P36 & P37	Averaged outlet exhaust gas temperature cylinders (Bank A & B)
P38 & P39	Turbocharger inlet exhaust temperature (Bank A & B)
P40 & P41	Turbocharger outlet exhaust temperature (Bank A & B)
P42	Turbocharger outlet exhaust pressure (bank A)
P43	Sea water pressure
P44	Main cooler inlet sea water temperature
P45	Main cooler outlet sea water temperature
P46	Main cooler inlet hot water temperature (engine outlet)
P47	Main cooler outlet hot water temperature (engine inlet)
P48	Hot water pressure
P49	Engine outlet lubricating oil temperature
P50	Lubricating oil pressure
P51	O_2 concentration dry in exhaust gas
P52	CO_2 concentration dry in exhaust gas
P53	CO concentration dry in exhaust gas
P54	NO concentration dry in exhaust gas
P55	NO_2 concentration dry in exhaust gas
P56	NO_x concentration dry in exhaust gas
P57	Engine room ambient temperature
P58	Engine room barometric pressure
P59	Engine room relative humidity

Thermodynamic failure modes

F1	Excessive pressure drop in air filter
F2	Efficiency reduction in air cooler
F3	Excessive pressure drop in air cooler
F4	Air compressor failure
F5	Intake air manifold leakage
F6	Intake valve seat failure
F7	Misfiring
F8	Excessive blow-by
F9	Failure of valve clearance adjustement - lower clearance -
F10	Failure of valve clearance adjustement - higher clearance -
F11	Injection timing failure – advance timing -
F12	Injection timing failure – delayed timing -
F13	Turbine failure

F14	Exhaust manifold leakage
F15	Excessive pressure drop in exhaust ducts

Sympthoms evaluated from engine model

S1	Boost pressure
S2	Air manifold temperature
S3	Cylinder outlet gas temperature
S4	Air mass flow
S5	IMEP
S6	Turbocharger RPM
S7	Compressor outlet temperature
S8	Exhaust manifold pressure
S9	Turbocharger inlet temperature
S10	Turbocharger outlet temperature

Latin symbols

t	Time	s
x	Flow longitudinal dimension	m
p	Pressure	pascal
e	Total internal energy	J
h	Total entalphy	J

Greek symbols

ρ	Density	kg m^{-3}
u	Velocity of fluid	m s^{-2}